Title:	Experimental investigation on fatigue of concrete cantilever bridge deck slabs subjected to concentrated loads
Authors:	Natário F., Fernández Ruiz M., Muttoni A.
Published in:	Engineering structures
DOI	10.1016/j.engstruct.2015.02.010
Volume: Pages:	89 pp. 191-203
Year of publication:	2015
Type of publication:	Peer reviewed journal article

Please quote as:	Natário F., Fernández Ruiz M., Muttoni A., *Experimental investigation on fatigue of concrete cantilever bridge deck slabs subjected to concentrated loads*, Engineering structures, 89, 2015, pp. 191-203.

Engineering Structures 89 (2015) 191–203

Contents lists available at ScienceDirect

Engineering Structures

journal homepage: www.elsevier.com/locate/engstruct

Experimental investigation on fatigue of concrete cantilever bridge deck slabs subjected to concentrated loads

Francisco Natário *, Miguel Fernández Ruiz, Aurelio Muttoni

Ecole Polytechnique Fédérale de Lausanne, ENAC, Station 18, CH-1015 Lausanne, Switzerland[1]

ARTICLE INFO

Article history:
Received 4 December 2014
Revised 27 January 2015
Accepted 10 February 2015

Keywords:
Shear strength
Model Code 2010
Critical Shear Crack Theory
Bridge deck slabs
Concentrated load
Fatigue behavior

ABSTRACT

Shear has been observed to be often the governing failure mode of RC cantilever deck slabs of bridges without shear reinforcement subjected to concentrated loads when tested under a quasi-static application of the load. However, concentrated loads of heavy vehicles have a repetitive nature, causing loss of stiffness and potential strength reductions due to fatigue phenomena.

In this paper, the fatigue behavior of cantilever bridge deck slabs is investigated. A specific experimental programme consisting on eleven tests under concentrated fatigue loads and four static tests (reference specimens) is presented. The results show that cantilever bridge deck slabs are significantly less sensitive to shear-fatigue failures than beams without shear reinforcement. Some slabs failed due to rebar fractures. They presented significant remaining life after first rebar failure occurred and eventually failed due to shear. The test results are finally compared to the shear-fatigue provisions of the *fib*-Model Code 2010 and the Critical Shear Crack Theory to discuss their suitability.

1. Introduction

Design of reinforced concrete cantilever bridge deck slabs without shear reinforcement is generally governed by the action of concentrated loads of heavy vehicles (Fig. 1), which may cause shear, punching shear or flexural failures. Amongst these potential failure modes, shear is the most common governing failure mode under quasi-static application of concentrated loads [1–4]. The concentrated loads resulting from heavy vehicles have a repetitive nature and may cause potential stiffness and strength reductions due to fatigue effects [5]. Fatigue failure modes are the same as the static ones and can be due to rebar fracture and/or failure of concrete.

Investigation of fatigue behavior in shear has mainly focused in the past on three and four-point bending tests on reinforced concrete beams without shear reinforcement (Fig. 2a). An extensive summary on this topic can be found in Ref. [6]. Beams can fail in bending or shear in both static and fatigue tests (bending failures being associated to rebar fracture or concrete crushing). Shear-fatigue failures were first studied by Chang and Kesler [7,8]. They observed two potential failure modes: *diagonal-cracking* failures (where failure takes place by development of a diagonal shear crack) and the *shear-compression* failures (where failure takes place when the propagation of the shear crack reduces the depth of the compression zone to an extent such that it can no longer resist the acting compressive forces).

However, it should be noted that the results obtained for beams and one-way slabs are not directly applicable to cantilever slabs subjected to concentrated loads. This is justified as beams do not exhibit a two-way action and consequently cannot redistribute their internal forces due to bending and shear cracking [4]. Moreover, the ratio between the maximum acting moment m_{max} and the maximum acting shear force v_{max} in cantilever slabs at the support is lower than for cantilever beams with the same shear span [2].

With respect to fatigue testing of reinforced concrete slabs without shear reinforcement under concentrated loads, previous research has mainly focused on simply supported or inner slabs [9–19] supported on two or four edges, refer to Fig. 2b and c. Table 1 presents some geometric properties of available experimental evidence. With respect to typical deck slabs of concrete bridges, it can be observed that several specimens have relatively low thicknesses (< 100 mm) and others have low reinforcement ratios ρ ($\leqslant 0.2\%$, including specimens even with no flexural reinforcement) or fairly large ones ($> 1.5\%$).

To the author's knowledge no tests are available on cantilever deck slabs (Fig. 2d), whose mechanical behavior may significantly differ from simply supported slabs [4]. In order to provide such experimental evidence, an experimental programme has been performed at the Ecole Polytechnique Fédérale de Lausanne (Switzerland). The specimens are full-scale slabs (3.00 m × 3.00 m × 0.25 m) with a central line support and subjected to a single

[1] http://ibeton.epfl.ch.

* Corresponding author.
E-mail address: francisco.natario@epfl.ch (F. Natário).

http://dx.doi.org/10.1016/j.engstruct.2015.02.010
0141-0296/

Notation

β	load reduction factor
δ	vertical displacement
ε	strain
ε_{max}	maximum strain
ε_{min}	minimum strain
ρ	reinforcement ratio
ϕ_{rebar}	reinforcement bar diameter
E_c	Young's modulus of concrete
F	applied force
F_{max}	maximum applied force
F_{min}	minimum applied force
F_{Ref}	quasi-static strength
LL	level of load
N	endurance
R	fatigue loading ratio
R_l	linear reaction force
S	stress level
V_{CSCT}	quasi-static shear strength according to the CSCT
V_{max}	maximum applied shear force
V_{max}^{tot}	maximum applied total shear force
V_{MC2010}	quasi-static shear strength according to the *fib*-Model Code 2010
V_{Ref}	quasi-static shear strength
V_{tot}	total shear force
a	shear span (distance between the center of the support and the center of the loading plate)
a_v	free shear span (distance between the edge of the support and the edge of the loading plate)
b	subscript indice representing "bottom"
d	effective flexural depth
d_g	maximum aggregate size
f_c	compressive strength of concrete measured in cylinders
$f_{c,Ref}$	compressive strength of concrete in reference tests
$f_{c,fat}$	compressive strength of concrete measured in fatigue tests
f_u	ultimate stress of steel
f_y	yield stress of steel
m_{max}	maximum acting unitary bending moment
t	subscript indice representing "top"
x	x-axis and coordinate
w_{cr}	crack opening
$w_{cr,max}$	maximum crack opening
$w_{cr,min}$	minimum crack opening
v_{max}	maximum acting unitary shear force
y	y-axis and coordinate

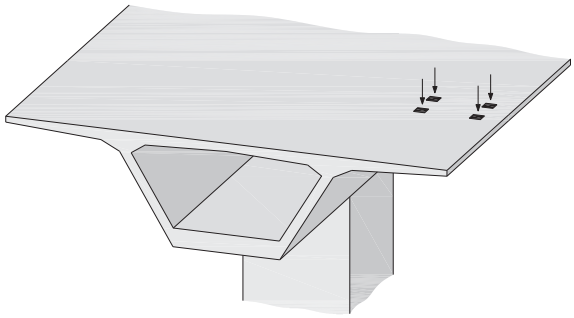

Fig. 1. Cantilever bridge deck slab subjected to concentrated loads.

concentrated load on both sides of the support. Four static tests were performed on two slabs (two tests per slab and load location) and eleven fatigue tests on eight slabs (four slabs per load location).

Other topics as the influence of moving loads [14,15,19] or the influence of impact loading on shear strength [20] are not investigated within this paper.

2. Test campaign

2.1. Test specimens

Ten slabs (FN1-FN10) were tested. The slabs had the dimensions of 3.00 m × 3.00 m × 0.25 m and contained only flexural reinforcement.

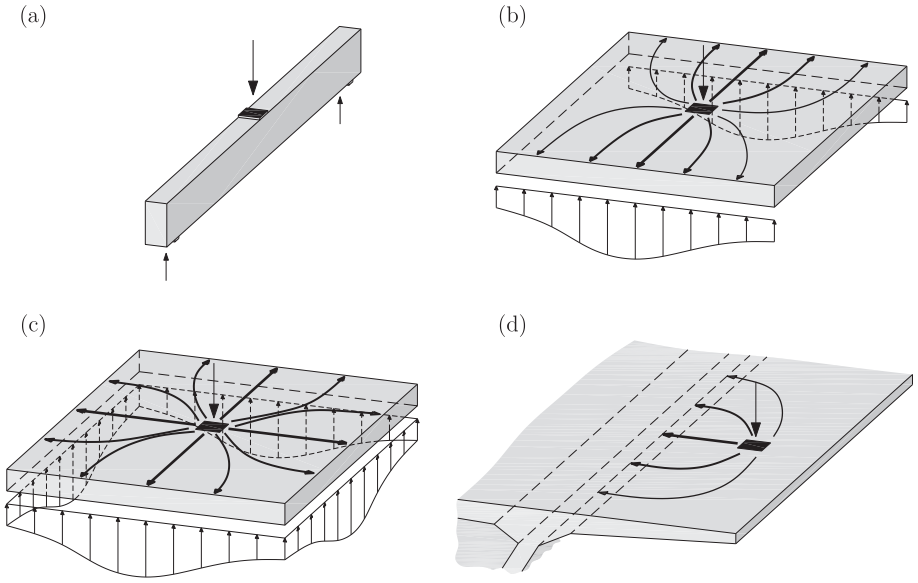

Fig. 2. Structural reinforced concrete members failing in fatigue shear loading: (a) simply supported beam; (b) slab supported on two edges; (c) slab supported on four edges; and (d) cantilever slab.

The geometry and reinforcement layout were the same for all slabs. The bending top reinforcement in the x-transverse direction (perpendicular to the support) consisted of 20 mm diameter bars spaced 150 mm with a nominal effective depth $d_{xt} = 210$ mm (nominal reinforcement ratio $\rho_{xt} = 1.00\%$), and the bottom one 16 mm diameter bars spaced 150 mm with a nominal effective depth $d_{xb} = 212$ mm ($\rho_{xb} = 0.63\%$). In the longitudinal direction, the top reinforcement consisted of 12 mm diameter bars spaced 150 mm ($d_{yt} = 194$ mm, $\rho_{yt} = 0.39\%$) and the bottom one 10 mm diameter bars spaced 150 mm ($d_{yb} = 199$ mm, $\rho_{yb} = 0.26\%$), refer to Fig. 3.

2.2. Material properties

Normal strength concrete was used in all slabs. Table 2 presents the compressive strength and modulus of elasticity (measured on concrete cylinders, 320 mm high, 160 mm diameter), as well as the age of concrete at the time of testing of the slabs. The compressive strength ranged from 32.3 MPa to 46.6 MPa and the modulus of elasticity from 28,000 MPa to 35,000 MPa. One cubic meter of concrete had a nominal composition of 832 kg of sand, 378 kg of gravel ranging between 4 and 8 mm, 681 kg of gravel ranging from

Table 1
Properties of slabs tested under concentrated fatigue loads.

Tests	ρ[%]	Thickness [mm]	Supports	Spans [cm]	Widths [cm]	Type[a]
Sawko and Saha [9]	–	38	Two edges	229-152-114	152	PC
Sawko and Saha [9]	1.7	76	Two edges	114	152	RC
Hawkins [10]	1.3	127	Two edges	122	127	RC
Batchelor et al. [11]	0.0–0.2–0.4–0.6	22-18-12	Two edges	30	305	RC
Okada et al. [12]	1.1–1.3	170-180	Four edges	235-360	–	RC
Sonoda and Horikawa [13]	1.3	60	Four edges	80-250	–	RC
Perdikaris and Beim [14]	0.0–0.3–0.7	32	Two edges	32	230	RC
Perdikaris et al. [15]	0.0–0.3–0.4–0.7	72	Two edges	71	170	RC
Youn and Chang [16]	1.0	60	Two edges	70	210	RC
Toutlemonde and Ranc [17]	1.2	180	Two edges	250	500	RC
Graddy et al. [18]	3.2	191	Two edges	183	213	RC
Hwang et al. [19]	–	115	Two edges	270	430	PC

[a] RC – reinforced concrete; PC – prestressed concrete.

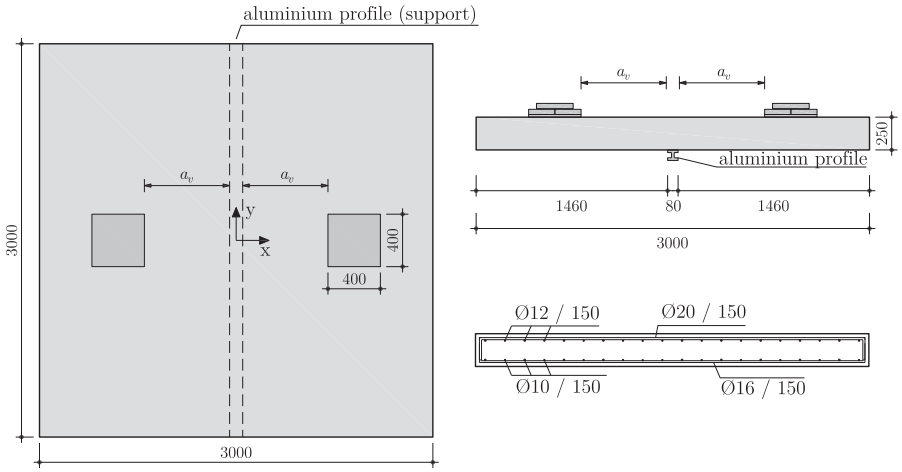

Fig. 3. Geometry and reinforcement layout of tested slabs (dimensions in [mm]).

Table 2
Properties of test specimens.

Slab	Side	a_v [mm]	Type of test	Age (start–end)	f_c (start–end)	E_c (start–end)
FN1	W	440	Static	129	45.2	33,000
FN1	E	440	Static	186	46.6	34,000
FN2	W	440	Fatigue	97–112	38.2–38.7	30,500
FN2	E	440	Fatigue	97	38.2	30,500
FN3	W and E	440	Fatigue	96–98	36.2	30,000
FN4	W	440	Fatigue	102–110	38.4–38.6	30,500
FN4	E	440	Fatigue	102	38.4	30,500
FN5	W and E	440	Fatigue	34–63	32.3–34.8	28,000–29,500
FN6	W	680	Static	144	45.7	33,000
FN6	E	680	Static	178	46.5	34,000
FN7	W and E	680	Fatigue	322	44.8	35,000
FN8	W	680	Fatigue	298–325	43.5–43.7	34,500
FN8	E	680	Fatigue	298–476	43.5–44.6	34,500–35,000
FN9	W and E	680	Fatigue	305–316	44.7	35,000
FN10	W and E	680	Fatigue	328–396	43.7–44.2	34,500–35,000

Table 3
Mechanical properties of the reinforcement.

Slab	ϕ_{rebar} [mm]	f_y [MPa][a]	f_u [MPa]	Type
FN1, FN6, FN7, FN8, FN9, FN10	20	579	680	Quenched and self-tempered
	16	553	650	Quenched and self-tempered
	12	520	620	Quenched and self-tempered
	10	504	595	Quenched and self-tempered
FN2, FN3, FN4, FN5	20	600	700	Quenched and self-tempered
	16	595	709	Quenched and self-tempered
	12	523	591	Cold-worked
	10	543	606	Cold-worked

[a] Offset yield-point at 0.2% strain for cold-worked rebar.

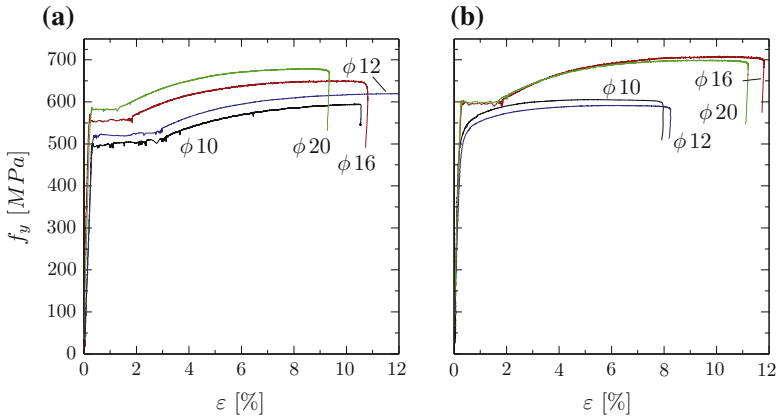

Fig. 4. Measured stress–strain relationships of reinforcement bars: (a) FN1, FN6, FN7, FN8, FN9 and FN10; and (b) FN2, FN3, FN4 and FN5.

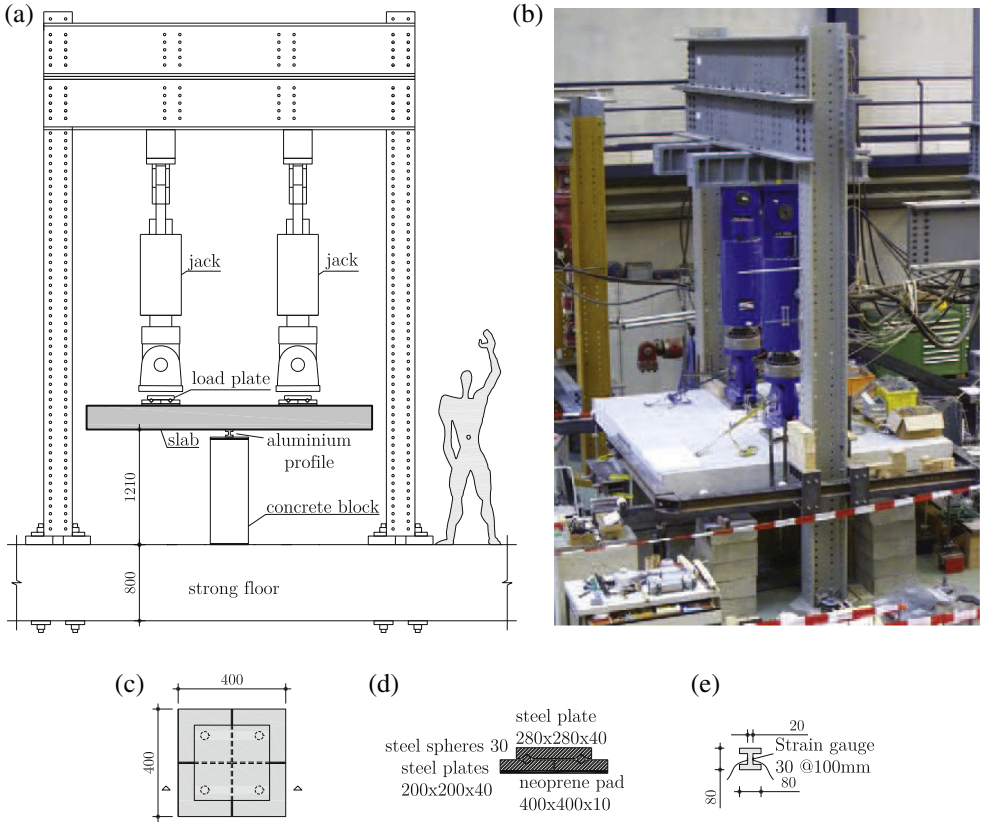

Fig. 5. Test setup (dimensions in [mm]): (a) side view; (b) picture; (c) loading plate plan view; (d) loading plate section cut; and (e) cross-section of aluminum profile.

8 to 16 mm, 310 kg of Portland cement and 111 kg of water. The maximum size of the aggregate d_g was 16 mm for all specimens.

Conventional reinforcing bars were used in the specimens. The average reinforcement mechanical properties of 3 tests per diameter are presented in Table 3 and the stress–strain relationships in Fig. 4.

2.3. Test setup

The test setup is shown in Fig. 5. The specimen was supported in the middle by means of a 80 mm I-shaped aluminum profile. On each side of the web of the profile, 30 strain gauges were glued with a 100 mm spacing (refer to Fig. 5e) to record the vertical strains of the profile and consequently the reaction forces, calculated by assuming an elastic behavior of the aluminum and considering a constant strain at the contributing area of each gauge. Reasonable agreement was found between the total measured reaction and the total applied force, with relative errors at maximum load of less than 15% for all tests. At the interface between the aluminum profile and the tested slab there was a thin layer of plaster of about 3 mm, in order to level the surfaces.

The loads were introduced by means of two hydraulic actuators fixed on a steel frame connected to the strong floor of the laboratory. The loading area was 400 mm × 400 mm in-plane and load was applied through a 10 mm thick neoprene pad. Each load was introduced in this area by means of four 200 mm × 200 mm × 40 mm steel plates, loaded in turn by a 280 mm × 280 mm × 40 mm steel plate. Between the top and bottom plates, steel spheres (30 mm diameter) were placed at the center of the bottom plates (Fig. 5c and d). This device was designed in order to distribute the load as uniformly as possible over the square contact area and is consistent to the dimensions of the fatigue load model of EN1991-2 for road bridges [21].

Two different loading locations were investigated, corresponding to a clear distance from the line support (a_v) of 440 mm and 680 mm (Fig. 3), corresponding to $2.1d$ and $3.2d$ respectively, where $d(= d_{xt})$ is the nominal effective depth of the slab.

After failure occurred on one side of the slab, that side was strengthened using steel external profiles and plates bolted on top and bottom faces, by means of prestressed bars. After strengthening, the test was continued leading to a second failure on the other side.

2.4. Test procedure

Two slabs were tested quasi-statically in order to obtain the reference static strengths (F_{Ref}) for each location of the load. Each slab provided two reference tests (duplicated values).

The fatigue loading was done in a combined force–displacement control mode. The forces of the two actuators were controlled taking advantage partially of the symmetry conditions of the test. The average force of both jacks was kept constant and both forces corrected to keep the relative displacement between them lower than 10 mm. Differences between maximum applied forces on both sides were lower than 1% for five tested slabs (FN3 and FN7–FN10), between 2–3% for two other slabs (FN2 and FN4), and 3.1% for the remaining one (FN5).

The target ratio R between the minimum (F_{min}) and the maximum (F_{max}) applied forces was 0.10, and the actual values varied between 0.09 and 0.12, refer to Table 4. These values are reasonable as in actual bridge deck slabs the ratio R of the traffic load is 0.0, yet dead load is also acting. A qualitative representation of the fatigue loading history is given in Fig. 6.

For each load location four different levels (LL) of maximum applied load were used. The maximum applied load was corrected in order to account for small differences of concrete compressive strength between fatigue and reference tests as follows:

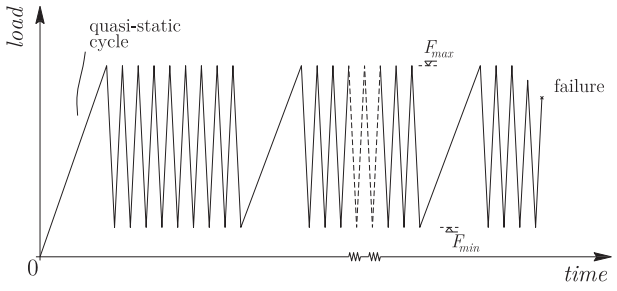

Fig. 6. Qualitative fatigue loading history.

Table 4
Main properties of tested specimens.

Slab	Side	a_v [mm]	Type	F_{max} [kN]	F_{min} [kN]	R	Actual LL [%]	Cycles N	Measured d_{xt}[mm][a]	Measured d_{yb} [mm][b]	Failure mode
FN1	W	440	Static	591	–	–	–	1	203	201	Shear
FN1	E	440	Static	597	–	–	–	1	203	201	Shear
FN2	W	440	Fatigue	520	53	0.10	96	1350	212	209	Shear
FN2	E	440	Fatigue	506	54	0.11	93	990	212	209	Shear
FN3	W	440	Fatigue	473	48	0.10	90	72,340	214	203	Shear
FN3	E	440	Fatigue	472	48	0.10	90	72,340	214	203	Shear
FN4	W	440	Fatigue	467	47	0.10	86	17,300	208	209	Shear
FN4	E	440	fatigue	456	49	0.11	84	15,560	208	209	Shear
FN5	W	440	Fatigue	394	36	0.09	79	501,810	210	209	Rebar fracture
FN5	E	440	fatigue	382	44	0.12	77	501,810	210	209	Rebar fracture followed by shear
FN6	W	680	Static	474	–	–	–	1	190	201	Shear
FN6	E	680	Static	499	–	–	–	1	190	201	Shear
FN7	W	680	Fatigue	427	46	0.11	89	824	197	201	Shear
FN7	E	680	Fatigue	427	46	0.11	89	824	197	201	Shear
FN8	W	680	Fatigue	378	42	0.11	80	5007	210	201	Shear
FN8	E	680	Fatigue	376	42	0.11	80	5193	210	201	Shear
FN9	W	680	Fatigue	333	35	0.11	70	311,200	200	201	Rebar fracture
FN9	E	680	Fatigue	334	38	0.11	70	311,200	200	201	Rebar fracture followed by shear
FN10	W	680	Fatigue	281	30	0.11	59	734,760	199	199	Rebar fracture followed by shear
FN10	E	680	Fatigue	282	30	0.11	60	734,760	199	199	Rebar fracture followed by shear

[a] Average value measured in the middle region of the center transversal saw-cut.
[b] Average value measured in the region under the loading plates in the center transversal saw-cut.

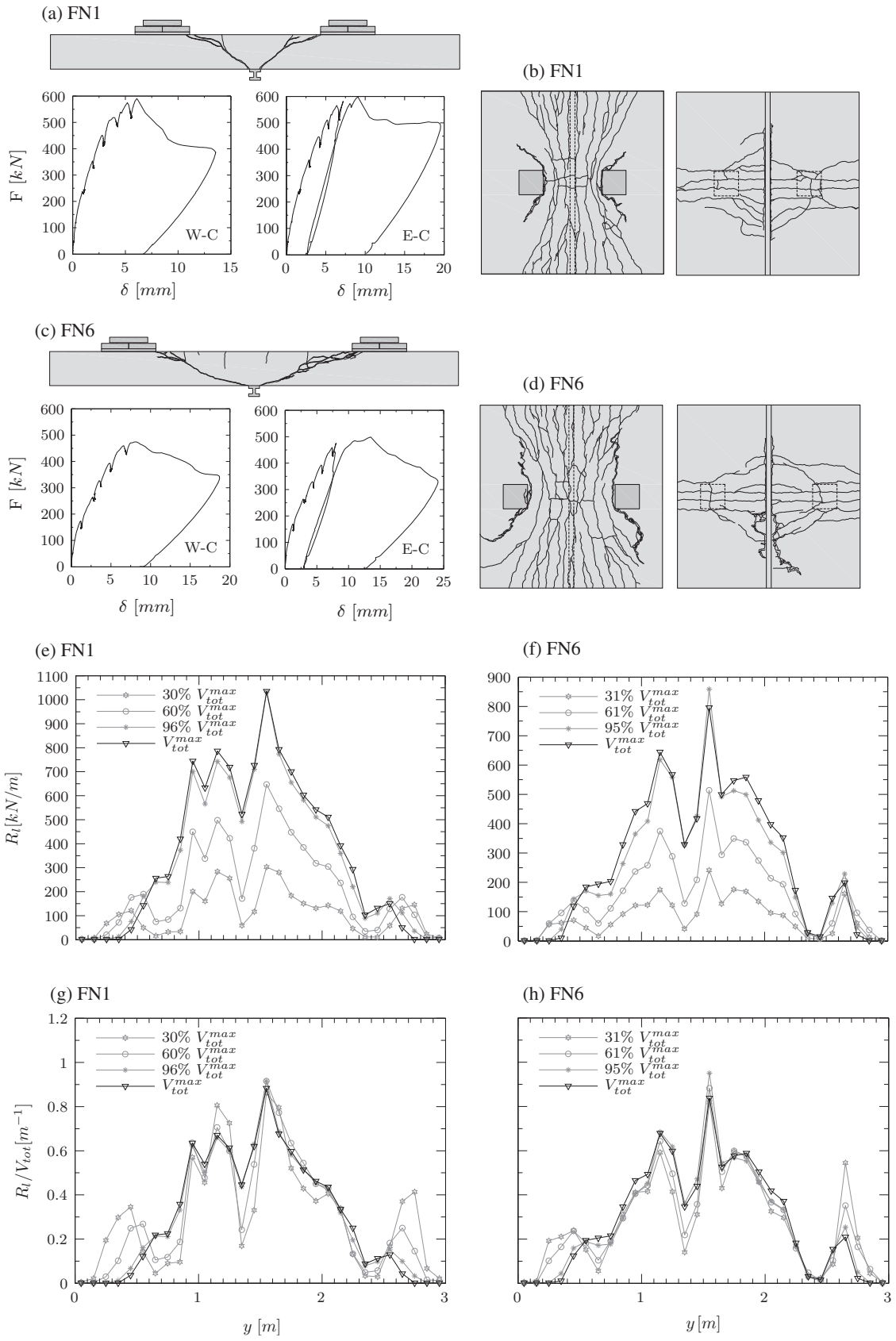

Fig. 7. Reference static tests: (a) central saw-cut and load deflection-curves at the center of the loading plates of slab FN1 ($a_v = 440$ mm); (b) top and bottom crack patterns of slab FN1; (c) central saw-cut and load deflection-curves at the center of the loading plates of slab FN6 ($a_v = 680$ mm); (d) top and bottom crack patterns of slab FN6; (e) measured linear reaction evolution in the first test of slab FN1; (f) measured linear reaction evolution in the first test of slab FN6; (g) normalized measured linear reaction evolution in the first test of slab FN1; and (h) normalized measured linear reaction evolution in the first test of slab FN6.

$$F_{max} = LL \cdot F_{Ref}\sqrt{\frac{f_c}{f_{c,Ref}}} \quad (1)$$

where F_{Ref} is the average static strength of the two reference tests, f_c is the concrete compressive strength at the day when testing started and $f_{c,Ref}$ is the average concrete strength of the two reference tests. For the free shear span $a_v = 680$ mm, the target loading levels LL were 60%, 70%, 80% and 90%, and for $a_v = 440$ mm 80%, 85%, 90% and 95%.

The fatigue loading was applied with a loading frequency of 1 Hz and for some specimens with 0.75 Hz and 0.5 Hz close to failure (FN9 and FN10, due to the required hydraulic debit of the actuators (related to the large displacements experienced by the slabs)).

2.5. Measurements

Continuous measurements were performed during the fatigue tests, namely the applied forces and the displacements measured by the actuators, thickness variation (up to fifteen points around each loading plate), the strains of selected rebars at some locations using strain gauges, and crack openings (up to ten locations) after the first loading cycle. In addition, measurements were taken in quasi-static tests at selected loading cycles (refer to Fig. 6), namely the aluminum profile strains (distribution of reaction forces) and the vertical displacements (up to fourteen points).

3. Test results

3.1. Static reference tests

The quasi-statically tested slabs (reference specimens) failed in shear, in a similar manner as the tests reported in [4]. Table 4 presents the maximum loads for all static tests. For both loading locations, once the maximum load was attained, the slabs presented a softening behavior, with a significant decrease of the applied load for increasing displacements (refer to Fig. 7a and c).

The crack pattern on the top surfaces developed parallel to the linear support in the central region, while on the bottom surface, cracking was mostly perpendicular to the support line and concentrated near the loading area, refer to Fig. 7b and d. The observed

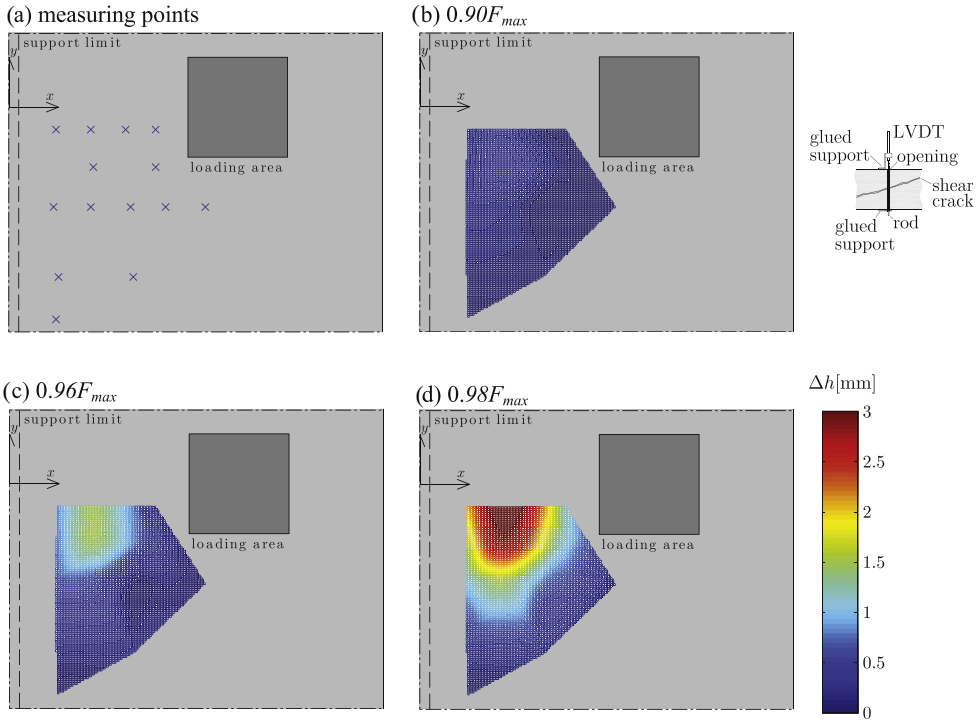

Fig. 8. Thickness variation in slab FN6 ($a_v = 680$ mm) side E: (a) measuring points; and (b–d) interpolated surfaces of thickness increases (in [mm]).

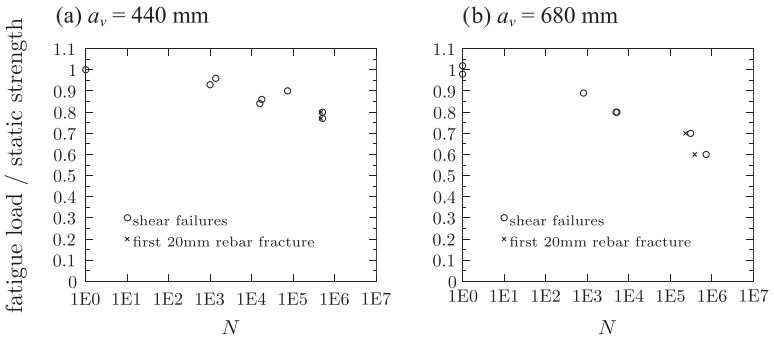

Fig. 9. Whöler diagrams of tested slabs: (a) $a_v = 440$ mm; (b) $a_v = 680$ mm.

failure crack in the central section of the saw-cuts (refer to Fig. 7a and c) was similar to shear cracking of beams (one-way slab strips) without shear reinforcement. For the largest shear span, the shear crack developed almost horizontally in the compression zone (soffit of the slab) near the edge of the support. In this case, the shear crack intercepted the top transverse reinforcement with a steep angle and at a distance approximately equal to d from the edge of the loading plate. The concrete cover spalled in this region due to dowel action of the main reinforcement. For the shorter shear span, the shear crack was steeper and straighter on average, also intercepting the upper main reinforcement at a distance approximately equal to d from the edge of the loading plate. The critical shear crack of both slabs seems to develop from a flexural crack at a certain distance from the loading plate (and not from the tip of the loading plate). Additionally it exhibits a horizontal branch close to the load due to dowel action, allowing to classify these failures as typical shear failures and not as punching failures around the load.

The reaction along the support line could be estimated (refer to Fig. 7e–h) based on the strain at each of the thirty locations of strain gauges of the I-shaped aluminum profile. As previously observed in a similar experimental series [4], close to failure the reaction in the central region increases at a lower rate or even decreases transferring the load to the adjacent regions. The level of load at which this phenomenon is observed is consistent with those observed for the development of the inclined shear crack, whose vertical opening is related with the increase of thickness of the slabs recorded during the tests, refer to Fig. 8 for a representative case. The figure also shows that the reaction tends to concentrate in the middle part of the support line as the applied force at the concentrated load increases (associated to the uplift of the extremities).

3.2. Fatigue tests

All slabs except FN5 ($a_v = 440$ mm; target $LL = 80\%$), FN9 ($a_v = 680$ mm; target $LL = 70\%$) and FN10 ($a_v = 680$ mm; target $LL = 60\%$) failed in shear-fatigue without rebar fractures. Table 4 presents the main results of the test campaign. Fig. 9 depicts the Wöhler diagrams for each loading position normalized by the average failure loads of the static reference tests. The ratio between the maximum applied loads (fatigue strength) and the static shear strengths are normalized with the square-root of the concrete compressive strength ($\sqrt{f_{c,Ref}/f_{c,fat}}$).

The slabs that failed in shear-fatigue presented similar crack patterns as the static reference specimens (refer to Figs. 10 and 11). The slabs which exhibited rebar fractures eventually failed in shear as well (except FN9-W), due to excessive flexural crack openings that propagated into critical shear cracks. This failure mode is similar to the shear failure observed after yielding of longitudinal reinforcement described in [22]. Tests with a free shear span $a_v = 680$ mm that failed with rebar fractures presented eight transversal 20 mm rebar fractures located at the top surface in

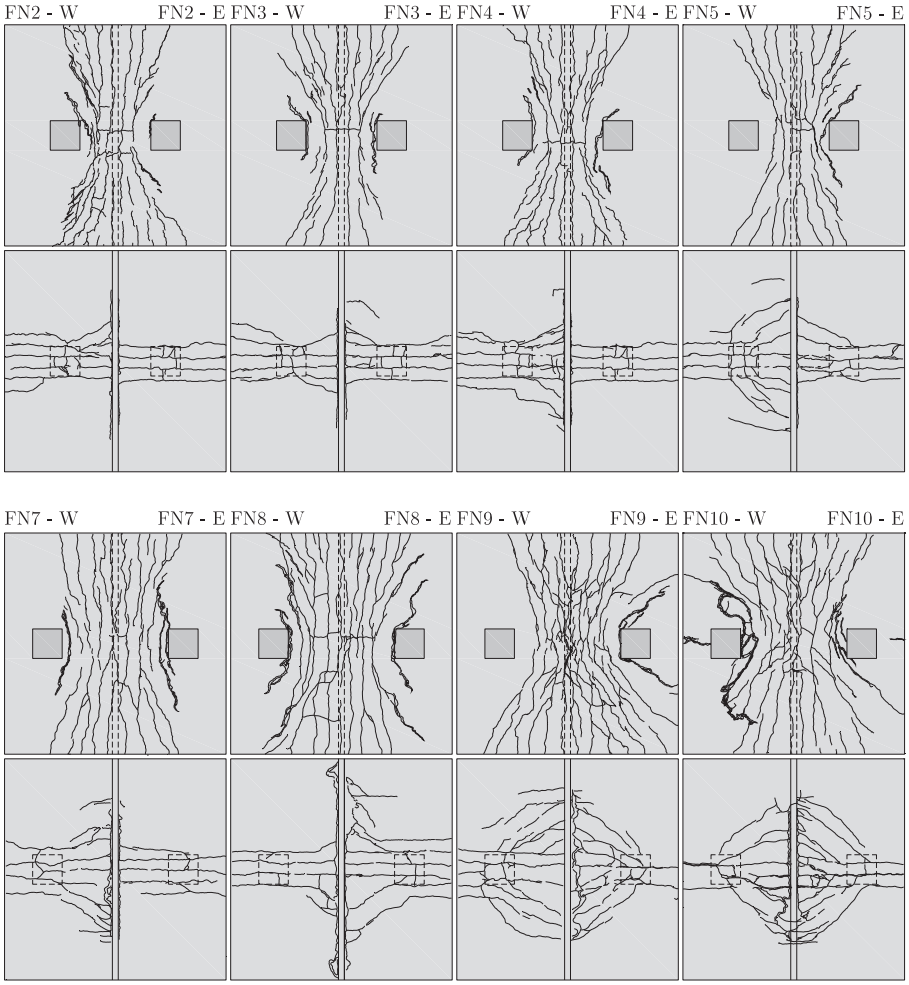

Fig. 10. Crack patterns: top and bottom faces.

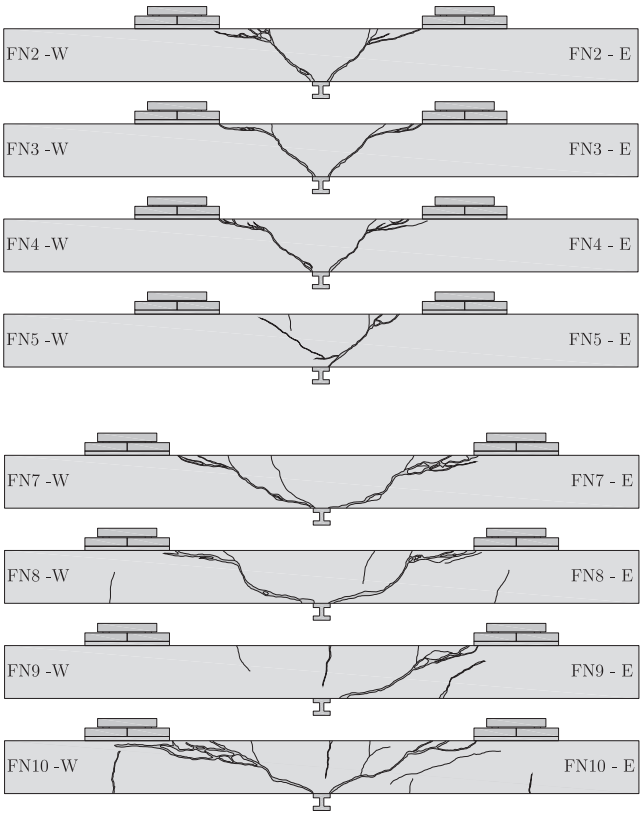

Fig. 11. Crack patterns: central saw-cuts.

the center line, as well as some 10 mm longitudinal rebar fractures on the bottom surface, developing a full flexural mechanism, refer to Fig. 12. The 10 mm bars are located at the transversal section that passes through the middle of the loading plates, between the load and the free edge.

The test with free shear span $a_v = 440$ mm which presented rebar fractures is somewhat different from previous cases. Three 20 mm rebars failed between the center line and one loading plate, at the intersection between the critical shear crack that developed from a flexural crack and the main flexural reinforcement, not developing a flexural mechanism. Dowel action might have generated additional stresses in the rebars due to local bending. This might have potentially contributed to an increase of the fatigue damage in these bars.

All bars failing under fatigue cycles were extracted from the tested specimens after failure to confirm fatigue failures, refer to Fig. 13.

Determining the cycle when the first 20 mm rebar failure took place was performed through cross-interpretation of the strain evolution measured in strain gauges placed at the center of some selected 20 mm rebars and the evolution of crack openings (devices to track crack opening evolution were placed at selected cracks after the first loading cycle), refer to Fig. 14 for two representative cases. When a top transversal 20 mm diameter rebar failed, the measured strain in the failed rebar diminished abruptly and the strain measurement in adjacent bars increased noticeably. This phenomenon could also be tracked by devices which measured crack openings in the vicinity of the failed bar, as a rebar failure contributes to larger crack openings. The determination of the cycle when the 10 mm bars failed was not possible. All slabs that failed due to rebar fractures presented a remaining life after the first 20 mm rebar fracture occurred. The slabs FN9 and FN10 ($a_v = 680$ mm) that developed a full flexural mechanism exhibited

Fig. 13. Failed rebars due to fatigue.

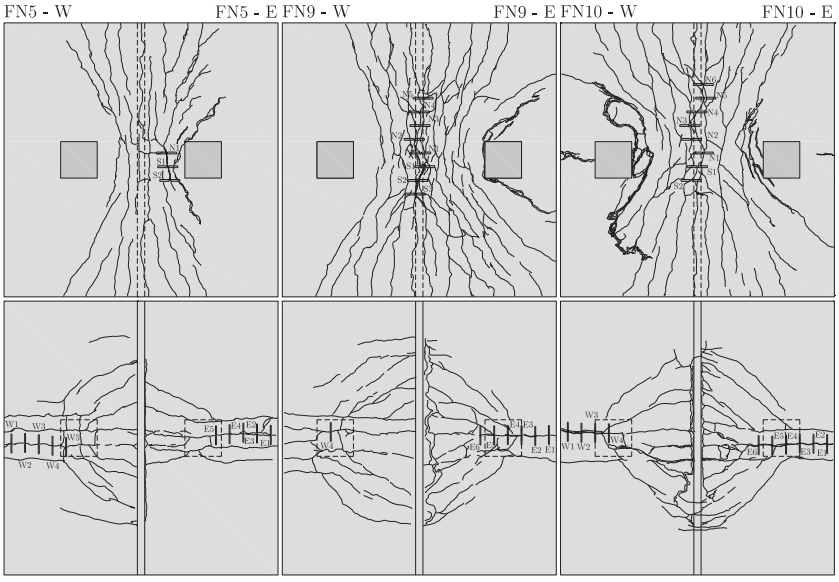

Fig. 12. Crack patterns and location of rebar fractures.

a significant one, 24.5% and 46.9% of the total endurance in this regime respectively, while FN5 ($a_v = 440$ mm) whose bars failed due to dowel action only had an additional 8.3% of the endurance in this state. It is relevant to note that the number of cycles until the first 20 mm rebar fracture for FN5 was approximately twice the number of FN9.

The fatigue loading led to progressive stiffness reductions for all tests. This phenomenon could be observed in the load–deflection evolution curves, refer to Fig. 15 for a representative case.

The linear reaction also varied with the fatigue loading. Close to failure, for both test types failing with or without rebar fractures, load transfer from the central region to the adjacent ones was observed, refer to Fig. 16 for a representative case. This is consistent with the observed results for quasi-static (reference) specimens near failure and confirms the capacity of these members to redistribute internal forces near failure.

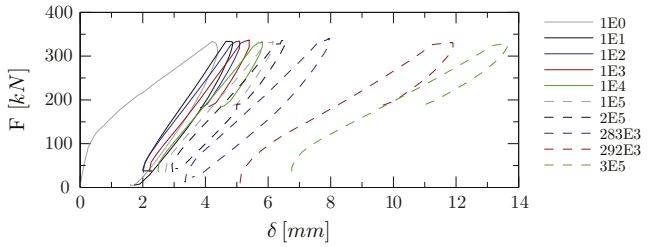

Fig. 15. Load–deflection evolution measured at the center of the loading plate of tested slab FN9-E ($a_v = 680$ mm).

4. Analysis of the test results

In the following, the results of the tests will be compared with the *fib*-Model Code 2010 [23] shear-fatigue provisions that depend

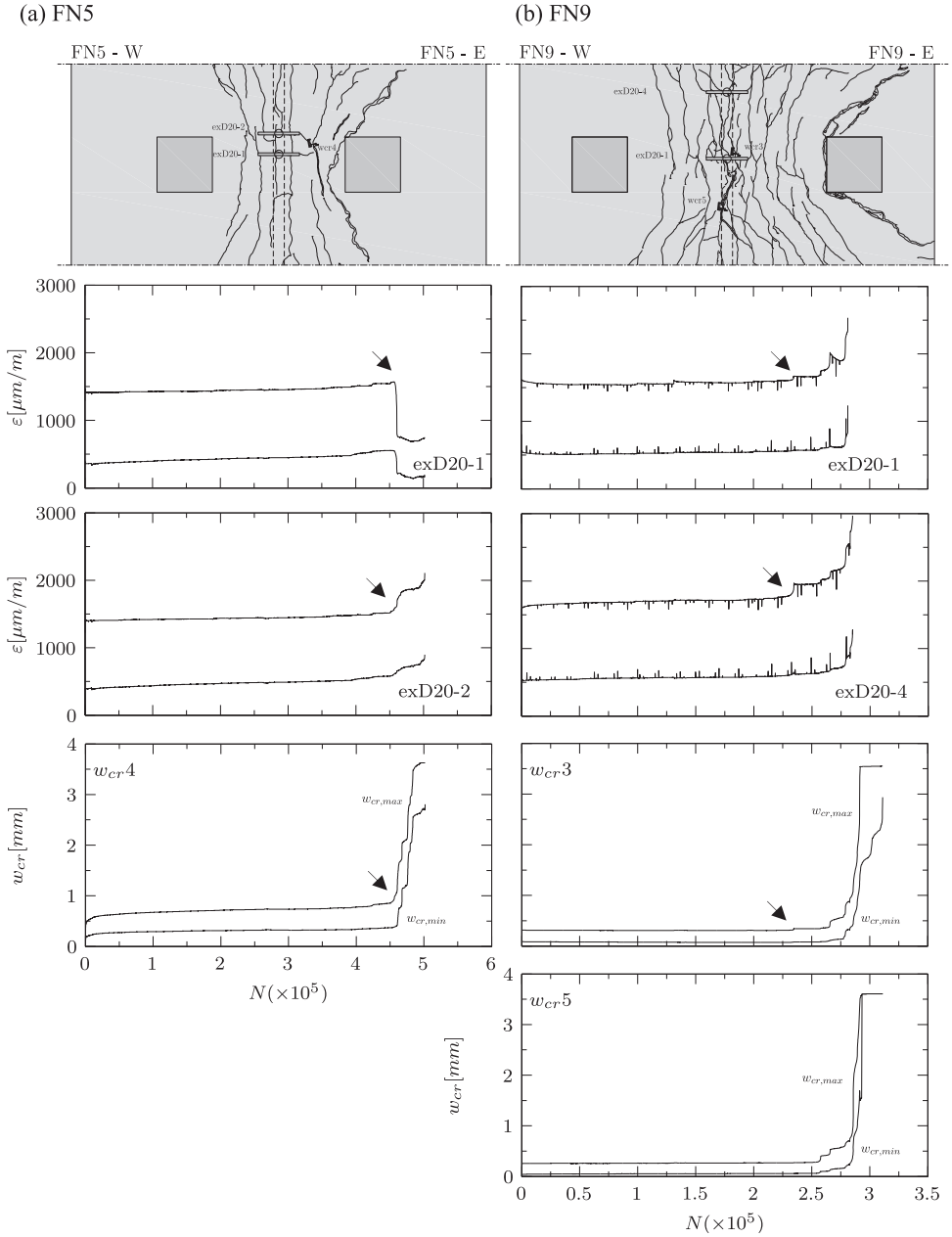

Fig. 14. Minimum and maximum measured strain evolution in the main transversal reinforcement and crack opening evolutions (maximum measurable value of approximately 3.5 mm): (a) FN5 ($a_v = 440$ mm); and (b) FN9 ($a_v = 680$ mm).

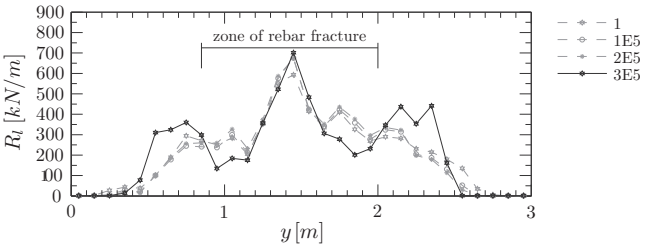

Fig. 16. Line reaction evolution of tested slab FN9 ($a_v = 680$ mm).

on the static shear strength. To that aim, the static shear strength will be calculated based on the *fib*-Model Code 2010 as well as using the Critical Shear Crack Theory (CSCT), as they are both based on mechanical models and allow a physical understanding of the observed phenomena [4].

First, a number of test results on statically determinate beams will be presented in order to understand the shear-fatigue behavior without any potential redistribution of internal forces. Such comparison with Eurocode 2 [24] approach can be found in [6]. Then, the results on cantilever slabs (with the potential to redistribute internal forces) will be compared.

4.1. *fib*-Model Code 2010 shear-fatigue provisions

The *fib*-Model Code 2010 proposes for reinforced concrete members without shear reinforcement the following *S*—*N* relationship between the endurance *N*, the maximum applied force V_{max} and the static shear strength V_{Ref} (refer to [4]):

$$\log N = 10(1 - V_{max}/V_{Ref}) \quad (2)$$

4.2. Fatigue tests on beams without shear reinforcement

Fig. 17 presents the comparison between the shear-fatigue provisions of the *fib*-Model Code 2010 and tests on beams without shear reinforcement that failed in shear-fatigue without rebar fracture [7,8,25–33]. The used database was created by Gallego et al. [6]. The reference static shear strength was calculated both with the *fib*-Model Code 2010 and the CSCT. Only tests with a distance between the centers of the support and of the load larger than three times the effective flexural depth are presented to avoid any potential arching action. These criteria lead to a reduction from 100 to 87 tests for the comparison with the *fib*-Model Code 2010 published by Gallego et al. [6].

Shear-fatigue failures on beams without shear reinforcement only seem to occur at maximum applied loads larger than approximately 50% of the static shear strength calculated according to both models. This is consistent with the threshold value proposed in EC-2 ($R = 0$) [24]. The shear-fatigue provision of the *fib*-Model Code 2010 is shown to be on the safe side when combined with the *fib*-Model Code 2010 static shear strength. The accuracy of the predictions is improved when the CSCT is used to estimate the quasi-static shear strength (V_{Ref}). This reduces the average (from 1.53 to 1.25) of the measured-to-predicted strength, yet keeping a constant value the Coefficient of Variation (0.23).

The linear law for shear-fatigue of the *fib*-Model Code 2010 (at logarithmic scale) seems to provide too safe estimates for an applied number of cycles larger than 100,000. From that number of cycles on, assuming a fatigue threshold of about 0.5 (as EC-2 for $R = 0$ [24]) seems more suitable, yielding an average of 1.38 (Coefficient of Variation of 0.15) for the *fib*-Model Code 2010 and 1.13 (Coefficient of Variation of 0.14) for the CSCT.

4.3. Static shear strength of beams and cantilever slabs

The shear strength of reinforced concrete beams without shear reinforcement according to the *fib*-Model Code 2010 is based on the Simplified Modified Compression Field Theory [34]. For cantilever slabs under concentrated loads, the control section is located at $d \leqslant a_v/2$ from the support and the shear force at that section is calculated by dividing the applied load by an effective width following a geometric rule [23]. Arching action is taken into account assuming that the contribution of point loads applied within a distance of $d \leqslant a_v \leqslant 2d$ from the face of the support to the design shear force may be reduced by the factor

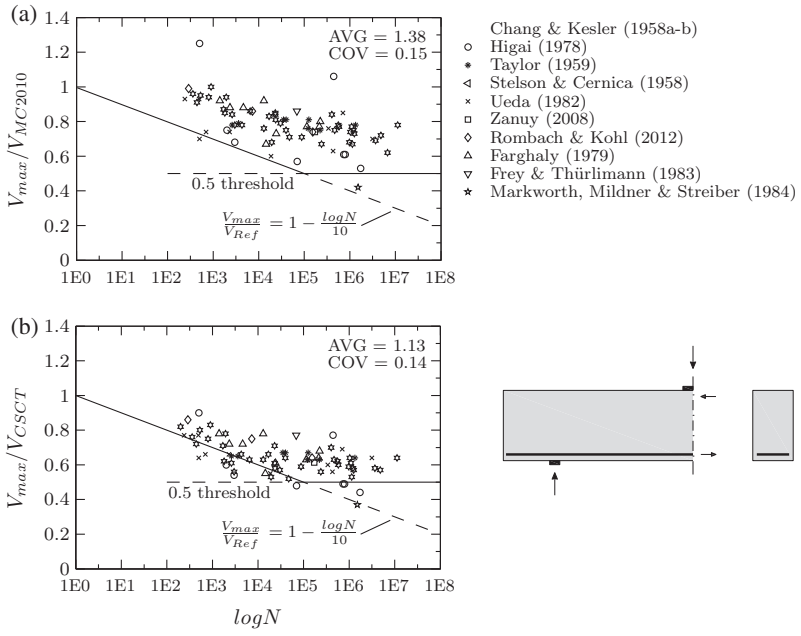

Fig. 17. Comparison between the *fib*-Model Code 2010 shear-fatigue provisions and the Wöhler diagram of tests on beams without shear reinforcement that failed in shear-fatigue without rebar fractures (database of Gallego et al. [6]), with the static shear strength calculated with: (a) MC2010; and (b) CSCT.

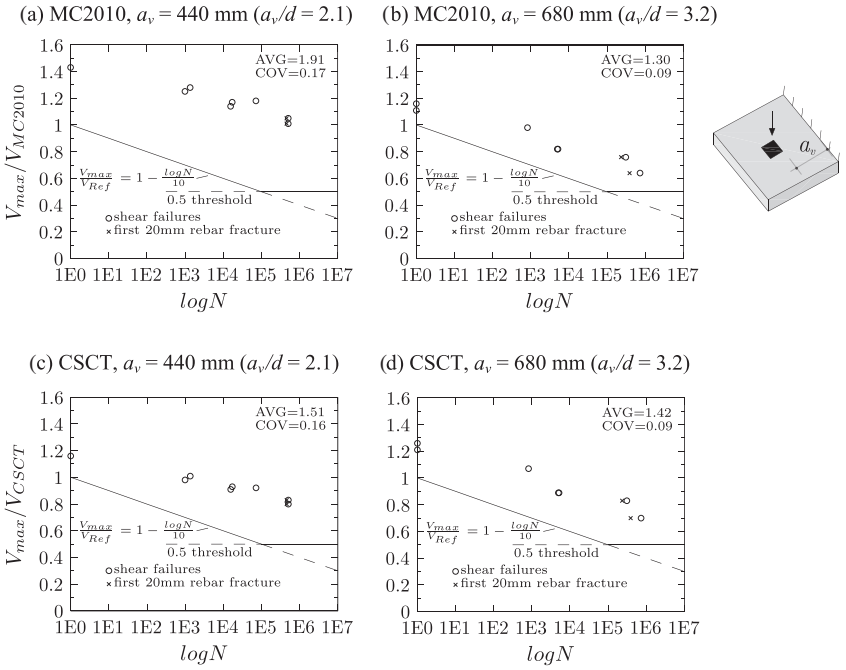

Fig. 18. Comparison between the *fib*-Model Code 2010 shear-fatigue provision (static shear strength calculated with the MC2010 and the CSCT) and the tested specimens: (a) MC2010, a_v = 40 mm; (b) MC2010, a_v = 680 mm; (c) CSCT, a_v = 440 mm; and (d) CSCT, a_v = 680 mm.

$$\beta = a_v/2d \leqslant 1 \tag{3}$$

The CSCT for reinforced concrete beams without shear reinforcement is thoroughly presented in [35]. The application of this theory to cantilever slabs subjected to concentrated loads is presented in detail in [4]. The acting shear force at the control section located at $d/2$ from the support is calculated on the basis of a linear elastic analysis and is averaged over a distance equal to $4d$ to take into account shear redistributions due to both bending and shear cracking [4]. Similarly to what has been reported for cantilevers subjected to distributed load [36], also arching action is considered for loads closer than $2.75d$ from the linear support:

$$\beta = a_v/2.75d \leqslant 1 \tag{4}$$

More details on how to apply these two approaches for cantilever slabs can be found in [4].

4.4. Tested cantilevers slabs

Fig. 18 presents the comparison between the shear-fatigue provisions of the *fib*-Model Code 2010 and the tested specimens, with the static shear strengths calculated with both the *fib*-Model Code 2010 and the CSCT according to [4]. The shear strength is underestimated by both approaches even in the quasi-static tests. This probably refers to the fact that the potential redistributions of shear forces (two-way action of the slabs) are estimated in an excessively conservative manner by the proposed effective distances where the shear force is averaged in both approaches. As the number of cycles increases, the safety margin seems to remain approximately constant (same slope for predictions and tests), indicating the pertinence of the shear-fatigue prediction and the presence of internal forces redistribution also for fatigue specimens. In addition, the test results seem to confirm that the *fib*-Model Code 2010 provides excessively safe estimates of the shear strength for loads acting close to the support ($a_v/d < 3$). This result is consistent with previous experimental investigations [4]. It can be noted that the values of maximum applied load were relatively high (60% or more of the static shear strength) and thus no fatigue threshold was observed.

5. Conclusions

This paper presents the results of an experimental programme on the fatigue behavior of reinforced concrete cantilever slabs subjected to concentrated loads near linear supports. The results are investigated and finally compared to the strength predictions of the *fib*-Model Code 2010 and the Critical Shear Crack Theory (CSCT). The main conclusions of this paper are:

- Fatigue loading of cantilever slabs with two-way action exhibits a similar influence on the shear strength as in beams (one-way slabs) without transverse reinforcement, decreasing the shear strength with increasing number of cycles.
- Redistribution of internal forces has been measured (by means of the reactions of the tested specimens) for cantilever slabs failing both under quasi-static and fatigue loading.
- The redistribution of forces enhances the shear strength of cantilever slabs with respect to equivalent beams in shear.
- Design models as the *fib*-Model Code 2010 or the CSCT seem to estimate in a safe manner the amount of internal force redistribution that potentially may develop, leading to conservative estimates of the actual shear strength.
- The *fib*-Model Code 2010 provides excessively safe estimates of the shear strength for loads acting close to support lines. This observation is consistent both for quasi-static and fatigue loading and indicates potentially an underestimate of the actual arching action.

Acknowledgements

The authors would like to gratefully acknowledge the support and funding of the Swiss Federal Road Authority and Dr. Juan Manuel Gallego for the kind permission to use his shear-fatigue database on beams without shear reinforcement.

References

[1] Vaz Rodrigues R, Fernández Ruiz M, Muttoni A. Shear strength of R/C bridge cantilever slabs. Eng Struct 2008;30:3024–33.
[2] Rombach G, Latte S. Shear resistance of bridge decks without transverse reinforcement (in German). Beton Stahlbetonbau 2009;104(10):642–56.
[3] Reissen K, Hegger J. Experimental investigations on the shear-bearing behavior of bridge deck cantilever slabs under wheel loads (in German). Beton Stahlbetonbau 2013;108(5):315–324,.
[4] Natário F, Fernández Ruiz M, Muttoni A. Shear strength of RC slabs under concentrated loads near clamped linear supports. Eng Struct 2014;76:10–23.
[5] CEB. Fatigue of concrete structures – state of the art report. Bulletin d'information 188; 1988.
[6] Gallego JM, Zanuy C, Albajar L. Shear fatigue behaviour of reinforced concrete elements without shear reinforcement. Eng Struct 2014;79:45–57.
[7] Chang TS, Kesler CE. Static and fatigue strength in shear of beams with tensile reinforcement. ACI J 1958;54(6):1033–57.
[8] Chang TS, Kesler CE. Fatigue behavior of reinforced concrete beams. ACI J Proc 1958;55(8):245–54.
[9] Sawko F, Saha GP. Effect of fatigue on ultimate load behavior of concrete bridge decks. ACI J Proc SP 1971;26–36:942–61.
[10] Hawkins NM. Fatigue design considerations for reinforcement in concrete bridge decks. ACI J 1976;73(9):104–15.
[11] Batchelor BdV, Hewitt BE, Csagoly P. An investigation of the fatigue strength of deck slabs of composite steel/concrete bridges. Transp Res Rec 1978:153–61.
[12] Okada K, Okamura H, Sonoda K. Fatigue mechanism of reinforced concrete bridge deck slabs. Transp Res Rec 1978(664):136–144,.
[13] Sonoda K, Horikawa T. Fatigue strength of reinforced concrete slabs under moving loads. Fatigue Steel Concr Struct 1982:455–62.
[14] Perdikaris PC, Beim S. RC bridge decks under pulsating and moving load. J Struct Eng 1988;114(3):591–607.
[15] Perdikaris PC, Beim SR, Bousias SN. Slab continuity effect on ultimate and fatigue strength of reinforced concrete bridge deck models. ACI Struct J 1989;86(4):483–91.
[16] Youn S-G, Chang S-P. Behavior of composite bridge deck slabs subjected to static and fatigue loading. ACI Struct J 1998;95(3):249–58.
[17] Toutlemonde F, Ranc G. Fatigue tests of cracked reinforced concrete slabs for estimating the service life of composite bridge decks. Rev Fr Gén Civ 2001;5(4):483–94.
[18] Graddy JC, Kim J, Whitt JH, Burns NH, Klingner RE. Punching-shear behavior of bridge decks under fatigue loading. ACI Struct J 2002;99(3):257–66.
[19] Hwang H, Yoon H, Joh C, Kim B-S. Punching and fatigue behavior of long-span prestressed concrete deck slabs. Eng Struct 2010;32:2861–72.
[20] Micallef K, Sagaseta J, Fernández Ruiz M, Muttoni A. Assessing punching shear failure in reinforced concrete flat slabs subjected to localised impact loading. Int J Impact Eng 2014;71:17–33.
[21] CEN. Eurocode 1: actions on structures – Part 2: traffic loads on bridges; 2003.
[22] Vaz Rodrigues R, Muttoni A, Fernández Ruiz M. Influence of shear on rotation capacity of reinforced concrete members without shear reinforcement. ACI Struct J 2010;107(5):516–25.
[23] fib. *fib*-Model Code 2010 – final draft, fib Bulletin 65, fib Bulletin 66, vols. 1 and 2; 2012. 350p., 370p.
[24] CEN. Eurocode 2: design of concrete structures – Part 1–1: general rules and rules for buildings; 2005.
[25] Higai T. Fundamental study on shear failure of reinforced concrete beams. Proc Jpn Soc Civil Eng 1978;1(279):113–26.
[26] Stelson TE, Cernica JN. Fatigue properties of concrete beams. ACI Spec Pub 1958;55(8):255–9.
[27] Taylor R. Discussion of a paper by Chang T.S., Kesler C.E. Fatigue behaviour of reinforced concrete beams. ACI J 1959;55(14):1011–5.
[28] Ueda T. Behaviour in shear of reinforced concrete beams under fatigue loading. Doctoral thesis. University of Tokyo; 1982.
[29] Zanuy C. Sectional analysis of reinforced concrete elements subjected to fatigue, including sections between cracks (in Spanish). Doctoral thesis. Universidad Politécnica de Madrid; 2008.
[30] Rombach G, Kohl M. Resistance of concrete members without shear reinforcement to fatigue loads. In: Proceedings of the IABSE conference innovative infrastructures – towards human urbanism; 2012.
[31] Farghaly SA. Shear design of reinforced concrete beams for static and repeated loads (in Japanese). Doctoral thesis. University of Tokyo; 1979.
[32] Frey R, Thürlimann B. Fatigue tests of RC beams with and without web reinforcement (in German). Report no. 7801-01. Institut für Baustatik und Konstruktion ETHZurich; 1983.
[33] Markworth E, Mildner K, Streiber A. Shear bearing capacity of RC beams under cyclic loads (in German). Die Strasse 1984;6:175–80.
[34] Sigrist V, Bentz E, Fernández Ruiz M, Foster S, Muttoni A. Background to the fib Model Code 2010 shear provisions – Part I: beams and slabs. Struct Concr 2013;14(3):204–14.
[35] Muttoni A, Fernández Ruiz M. Shear strength of members without transverse reinforcement as a function of critical shear crack width. ACI Struct J 2008;105(2):163–72.
[36] Pérez Caldentey A, Padilla P, Muttoni A, Fernández Ruiz M. Effect of load distribution and variable depth on shear resistance of slender beams without stirrups. ACI Struct J 2012;109(5):595–603.